

## Optical Multi-bead Arrays for Simple and Complex Odor Discrimination

**Keith J. Albert and David R. Walt\***

The Max Tishler Laboratory for Organic Chemistry, Department of Chemistry, Tufts University, Medford, MA 02155 \*Corresponding author for sensor work. Fax: 617.627.3443; Email: [david.walt@tufts.edu](mailto:david.walt@tufts.edu)

**Daljeet S. Gill and Tim C. Pearce\***

Department of Engineering, University of Leicester, Leicester LE1 7RH, United Kingdom \*Corresponding author for computational work. Tele: +44(0)116.223.1290 Fax: +44(0)116.252.2619; Email: [t.c.pearce@leicester.ac.uk](mailto:t.c.pearce@leicester.ac.uk)

### ABSTRACT

A fiber optic bead-based sensor array platform has been employed to discriminate between six different odors and air carrier gas. Six different bead sensor types, with over 250 replicates of each, were monitored before, during, and after odor exposure to produce time dependent fluorescence response patterns that were unique for each sensor-analyte combination. A total of 2683 sensors were analyzed with respect to changes in their fluorescence and signals from identical sensor beads were averaged to improve signal-to-noise ratios. 100% analyte classification rates were achieved for three complex (coffee bean) odors and three pure (simple) odors (toluene, acetone, and 1,3-dinitrotoluene) measured at their highest relative concentrations. When lower odor concentrations were employed, the system exhibited better than 85% classification rates for analyte discrimination. Sensor response repeatability to these odor stimuli has also been quantified statistically, which is vital in defining the detection limit of the overall system. These results demonstrate, for the first time, the utility of our bead array technology for discriminating between different odor types at various dilution levels.

### INTRODUCTION

Over the last two decades, there has been an increase in the development of odor detection systems that utilize cross-reactive sensor arrays in conjunction with pattern recognition techniques to interpret array response patterns.<sup>1-10</sup> These sensor array systems have been referred to, variously, as artificial, or electronic noses and are playing an increasing role as screening tools to complement existing analytical techniques. The development of odor detection systems is progressively moving towards systems that mimic, on some or many levels, the vertebrate's olfactory system. It is believed that the olfactory receptor neurons are cross-

sensitive and create neuronal response patterns<sup>11</sup> which are used as a basis for identifying aromas as pungent, putrid, flowery, etc. even though the components within the aroma are never quantified directly or individually identified. In the same way that mixtures of odor molecules create unique response patterns in the olfactory bulb, which the brain subsequently interprets as a particular odor quality, artificial nose systems rely on response patterns of physical or chemical molecular characteristics that can be attributed to an odor observation without knowing every component. In such systems, sensor-analyte response patterns are used to train statistical classifiers for subsequent odor interpretation, discrimination, and/or quantification.<sup>7-10</sup> This technology can be applied in situations where it is not necessary to know an odor's composition in detail<sup>12</sup> but are instead used to detect changes in odor characteristics even in a complex (sometimes interfering) background, i.e., such as monitoring the presence/absence of low-level explosives-like nitroaromatic compounds (NAC).<sup>13-16</sup> Classification of complex odors or odor environments is a much more difficult task because of overall odor complexity, e.g., coffee odors can contain hundreds of odorous compounds.<sup>17</sup> Despite the complex nature of some odors, sensor array systems have been able to discriminate between different types of coffee<sup>18-21</sup> and one such study determined the minimum number of sensors and transducers needed to obtain clear discrimination between three coffee brands and three mixtures of the brands.<sup>22</sup>

Here, we report on our use of a combined optical imaging and sensor array system to discriminate between six odor conditions, including three different coffee types, and air (control) carrier gas. The system is based on previously-developed cross-reactive array technology<sup>23,24</sup> and incorporates optical imaging fibers, which are high-density arrays of micron-scale optical fibers,<sup>25</sup> as our sensor platform. The imaging fiber's distal face is chemically etched to create an array of 'optically-wired' addressable microwells on the fiber's tip,<sup>26</sup> into which complementary-sized microsphere sensors are incorporated.<sup>27</sup> The microspheres have the solvatochromic dye Nile Red<sup>28-30</sup> adsorbed on their surface, which undergo intensity and/or wavelength shifts upon microenvironmental polarity changes. During odor exposure each sensor type produces a unique temporal fluorescence response profile depending on sensor-analyte interactions, i.e., odor polarity and diffusion. These sensor materials have been well documented for optically-based odor detection techniques.<sup>13-16,31</sup> This sensor array platform has recently been shown to detect low-level nitroaromatic compounds (NACs) in higher background

concentration levels of volatile organic compounds (VOCs) with 100% accuracy.<sup>14</sup> We now employ an array with more sensor types to show for the first time, that high-density arrays of cross-reactive bead sensors can detect and discriminate between simple and complex odors at various analyte dilutions. We also report on a new method for automatically analyzing sensor-analyte response profiles and for compensating for small shifts, e.g., array movement, within the source image. This new image analysis technique may eventually facilitate real-time monitoring, which is of paramount importance for many detection platforms employing image analysis (security, food quality, medicinal diagnostics, mine detection, etc.). Sensor response repeatability from run-to-run to the above odor stimuli have also been statistically quantified which is important since it limits the detection of the microsensor technology in a practical chemical sensing system.<sup>32</sup>

<Table 1>

<Figure 1>

## EXPERIMENTAL SECTION

**Materials.** Acetone, ethanol, and toluene were purchased from Fisher (Pittsburgh, PA). Nile Red dye, N-[3-(trimethoxysilyl)propyl]aniline, and 1,3-dinitrobenzene (DNB) were purchased from Aldrich (Milwaukee, WI) and used as received. Hazelnut, French Roast, and Columbian coffee beans (Jim's Organic Coffee) were used as purchased. The carrier gas used in the experiments is ultra zero grade air from Northeast Gas, Inc. (Salem, NH). A 1010 Precision Gas Diluter (tedlar-bag gas-dilution system) and analyte bags were purchased from Custom Sensor Solutions, Inc. (Naperville, IL). Tween 20 was obtained from J. T. Baker Chemical Company (Phillipsburg, NJ). The excitation filters employed were purchased from Chroma Technology Corp. (Brattleboro, VT). The pre-etched, optical imaging fibers (with 3.19 and 5.5  $\mu\text{m}$  core diameters) were purchased from Illumina, Inc. (San Diego, CA). Six different types of porous silica microsphere packing material were removed from HPLC columns (Phenomenex, Torrance, CA) and employed as substrates to which the fluorescent dye is physisorbed (**Table 1**).

**Bead sensor fabrication.** All sensors, except *B*, were prepared as described previously.<sup>13</sup> Briefly, the porous silica microspheres were rinsed thoroughly with ethanol and allowed to dry in room air overnight. Each microsphere type was individually stained with a solution of 0.5

mg/mL Nile Red in toluene by placing ~50 mg of microsphere material on a vacuum filtration system, rinsing with toluene, and then passing the Nile Red solution over the beads. Nile Red is readily sorbed to the surface of the modified porous silica microspheres and excess dye was removed by subsequent rinsing steps with toluene and deionized water. See Supporting Information for sensor *B* fabrication details. All beads were stored dry, except *C*. One day before data collection, approximately 30 mg *C* were added to a 1 mL 0.01% Tween 20 in deionized water.

**Array fabrication.** Six pre-etched, imaging fibers were employed and all sensors except *C* were distributed into the wells by a dry deposition process as shown previously.<sup>13</sup> Sensor *C* was deposited onto the fiber's etched face by removing 2  $\mu$ L bead/Tween 20 solution and placing onto the etched face. As the solution dried, the beads assembled spontaneously into the wells (one sensor per well). Excess beads were removed with a sharp burst of air from a dry air gun (2 s air pulse). The six fibers were separated into two groups of three fibers (bundle *A-C* & bundle *D-F*). Each group was bundled together with heat shrink tubing. To equally align the proximal ends of the bundle, each bundle was polished on an Ultra Tec Mfg., Inc. fiber polisher (Santa Ana, CA) with 30, 9, 3, 1 and 0.3  $\mu$ m lapping films.

**Instrumentation.** *Imaging & analyte delivery system.* Each fiber bundle was positioned onto a custom built imaging system with a vacuum-controlled sparging apparatus odor delivery system<sup>33</sup> as employed previously.<sup>24</sup> The imaging system employs an inverted Olympus fluorescence microscope incorporating a 75 W Xe excitation source with detection by a 640 x 480 pixel SensiCam high performance CCD camera (Cooke Corporation, Auburn Hills, MI). All testing events employed a 10x (NA 0.30) Zeiss microscope objective.

*Analyte Preparation.* To deliver the volatile organic compounds (VOCs), a tedlar-bag gas-dilution odor delivery system was employed as previously described.<sup>13</sup> Three tedlar bag analytes (air, acetone, toluene) were prepared by adding the proper amount of solvent analyte (none added for 'air') with a syringe needle into a flowing diluent air stream (see Supporting Information for sample bag preparation). Solid 1,3-dinitrotoluene (DNB), and different types of coffee beans, were individually placed in sealed flasks for odor delivery by a vacuum-controlled sparging apparatus. A second blank (air) sample consisted of an empty sealed flask which was purged with air carrier gas. It should be noted that analyte delivery was based on dilution of the saturated odor stream and not by employing calibrated vapor generators. The saturated vapor

pressure for 1,3-DNB (as used in this study for quantitative purposes) was 1 part per million (ppm).<sup>34</sup>

**Data Collection.** The CCD camera captures the fluorescence changes before, during, and after odor exposure to the sensor array by recording image sequences. Each sequence consisted of 45 images with 5 images (e.g., a baseline) captured before analyte delivery, 15 images captured during delivery, and 25 captured post-odor delivery. The total duration of each image sequence was 5.44 seconds with a odor exposure period of 1.81 seconds. Sixty five odor observations were recorded for each fiber bundle (bundle *A-C* and bundle *D-F*). All testing parameters were identical for each bundle except for the type of neutral density (ND) filter employed to decrease excitation light intensity. For bundle *A-C* and bundle *D-F*, 0.25 ND and 0.6 ND filters were employed respectively. The excitation and emission filters were 560 (bandpass 40) nm and 630 (bandpass 20) nm for both bundles. The CCD was binned 2 x 2 and employed 100 ms CCD exposure time. Total air flow was 250 mL/min and two different delivery systems were used together (a tedlar-bag system for acetone and toluene) and the sparging system for 1,3-DNB and the three coffee bean types. Responses from a total of 2683 sensors were analyzed, with different numbers of sensors used from each of the six types (see **Table 1**). The resulting fluorescence signals from identical sensors were combined and averaged to improve detection limits by decreasing the noise in the response. All experiments were performed at room temperature. Odor responses were recorded for all six analytes and the air carrier gas, for a total of sixty five observations (**Table 2**). The highest concentration level for each analyte (and air) was recorded five times in order to assess sensor response reproducibility from run-to-run. Five replicates at highest concentration x seven analytes (5 x 7 = 35 observations) plus five lower concentrations x six analytes (5 x 6 = 30 observations) totals sixty five observations.

**Image Processing.** All sixty five odor observations, each consisting of 45 CCD images, were divided into individual files, i.e., each odor sequence consisted of 45 individual image files. Image processing was conducted using Labview<sup>TM</sup> and IMAQ Vision<sup>TM</sup> (National Instruments, USA). A Virtual Instrument (VI) was programmed to automatically identify beads on the images based around the “IMAQ Circles” sub-VI that is able to fit circles within 2-D images using a least-square, best fit criterion.<sup>35</sup> A binary thresholding operation was carried out first on a selected image within the sequence of 45 images for each observation, in order to generate a

binary image required for circle fitting. A single Region Of Interest (ROI) could be specified on the selected image in order to identify the boundaries for a single bead type. After thresholding the image, the VI then fitted circles of variable radius to the image within the ROI. The threshold settings were then optimized for the image sequence in order to obtain the most accurate fitting of bead outlines (least squares) within this region. Once this was achieved each image within the sequence was processed using the same fitted circle data. For each identified bead the average grayscale count was calculated for each frame within the sequence. Care was taken to ensure that each bead could be tracked from image to image so that the intensity values could be compared directly between image sequences. In this way it was possible to accurately assess the response from individual beads across the entire collection of image sequences. **Figure 1** shows the final fitted circles for each of the six bead types superimposed on the original grayscale images.

By checking the baseline value for a single bead (the average grayscale count before exposure to the analyte) across all of the sequences we identified some irregularities in the images. On closer inspection it was clear that a very small amount of movement (1-2 pixels in the x or y direction) had occurred between the camera and the fiber bundle at specific points during the data collection – an inevitable consequence of the length of time and logistics of operating the equipment. This movement was digitally compensated for by adding software capability to offset the fitted circle data so as to match the newly relocated bead positions. This arrangement managed to completely remove the discontinuities in the baseline value from test-to-test. The individual bead response profiles were averaged over all beads of a single type to produce a temporal response profile for each bead type during the 45 image sequence.

<Table 2>

## RESULTS & DISCUSSION

In this paper, for the first time, an array of six different Nile Red stained porous silica beads was employed to monitor and discriminate between simple and complex odors at various dilutions. **Table 1** shows each sensor's composition and the representative population for each of the six sensor types. To simplify the identification of each bead type, we incorporated each microsensor type into the microwells of six different imaging fiber arrays so that each array

contained replicates of one sensor type, i.e., each of the six fiber arrays contained replicates of only one of the six bead types. The imaging fibers were then bundled together to create multi-bead sensor arrays composed of hundreds to thousands of individually addressable micron-sized sensor elements (**Figure 1**). The use of the microsphere sensors permits large quantities of sensors to be deployed in a small area, e.g., each imaging fiber's face is 1 mm<sup>2</sup> and can consist of tens of thousands of individually addressable sensor elements. More than 250 copies of each sensor type are represented (**Table 1, Figure 1**) and response profiles were recorded before, during, and after odor exposure with a CCD camera for six analytes and also for air carrier gas (**Table 2**). Sensor response profiles from identical sensor elements for each of the six sensor types were averaged to increase the S/N ratio as shown previously.<sup>13,31</sup> By averaging individual sensor responses, signal-to-noise (S/N) ratios increase and the array's overall dynamic range improves for lower level odors.<sup>13,31</sup> The sensor-analyte response profiles develop immediately upon odor exposure and the system's rapid response time<sup>13</sup> is progressing towards real-time detection. The sensor-analyte response profiles for each bead were analyzed using Labview<sup>TM</sup> and IMAQ Vision<sup>TM</sup> processing software (see Experimental). Briefly, the CCD sequence for each analyte observation was separated into individual image files and analyzed with respect to fluorescence changes over time for designated sensor elements. The concentration range for 1,3-DNB was 100-900 ppb and each VOC concentration ranged from 450-9000 ppm. The sensors were exposed to six dilution levels for each of the six odors and the highest relative dilution level for each odor was repeated five times. Including five air (blank) responses, 65 odor observations were examined. Although the number of observations is low, the total number of sensors employed is very high, i.e., each sensor's response profile can be considered to be an independent observation. A CCD was employed because it permits many sensor types to be monitored simultaneously and allows uncorrelated noise to be removed by monitoring responses from many individual sensor elements.<sup>13</sup>

*Preprocessing Methods.* After obtaining each individual sensor element's response over every frame within the series of CCD images, the fluorescence intensity values were averaged over all the identical sensor elements in order to produce a time-dependent response for all six bead types. **Figure 2** shows the averaged normalized response profile for each bead type during a single test sequence to each type of odor stimulus. These data show rapid responses with good reversibility, although the bead responses to both DNB and Hazelnut coffee odors were

noticeably slower in recovering to their original (baseline) values (**Figure 2d and 2e**). Four of the six bead types (*A*, *D*, *E*, *F*) show polarity changes in their response profiles to different odors, i.e., sensor responses show an increase or decrease in fluorescence intensity depending on the analyte, providing valuable additional diversity in the array response as a whole. The other two sensor types did not show polarity changes in their response profiles for the odors tested. Standard pre-processing metrics including fractional, relative, difference, array normalized, and sensor autoscaled (these methods have been detailed widely<sup>3,36</sup>) were used in order to extract a single time-independent parameter for each sensor-analyte combination. Subsequent data processing was conducted for each of these pre-processing metrics in order to reduce bias in the results and permit a quantitative comparison between the metric types.

<Figure 2>

*Exploratory Data Analysis.* Radar plots were used to illustrate interclass variation in the bead responses to the highest analyte concentration. Radar plots for the fractional grayscale metric with percentage response from the initial grayscale baseline values for each of the six bead types to the six odor conditions and air carrier gas are shown in **Figure 3**. The fractional values range between -5% (for toluene) to +8% (for acetone). In order to assess the repeatability of the bead responses, five repeated observations were recorded for each odor class (at maximum concentration). **Figure 3** shows the mean of the five highest concentration observations for each class (central solid line) as well as 1 standard deviation (SD) either side of the mean (outer dashed lines), indicating the reproducibility of response for each bead type to each odor class. Interestingly, the radar plots indicate that this reproducibility depends upon the odor stimulus. For example, bead type *D* shows good reproducibility to air, toluene, acetone, 1,3-DNB, Columbian coffee and French Roast coffee beans (**Figure 3a, 3b, 3c, 3d, 3f, and 3g**) but less reproducibility to Hazelnut coffee beans (**Figure 3e**). In general, this kind of observation may be due to some irreversible or temporary poisoning effect between specific odors and the bead type. It is likely that some of the observed response profiles may be less dependent on the concentration of analyte and more dependent on each analyte's relative activity for that sensory material.<sup>37</sup> In this study, odor classifications were not based on analyte concentration because, as shown in **Table 2**, at least two odors (toluene, acetone) were at the same level for each

exposure. We can discriminate between different odor classes even at different concentration levels, so discrimination cannot be based upon different concentration levels alone, but must be due to other analyte properties. Every odor class produced significant response profile differences in at least one of the six bead types, which was a good preliminary indication for potential classification between observations, and in general represents a trivial classification problem for each analyte's highest concentration level. Principal Components Analysis (PCA) was used as the standard technique to reduce the dimensionality of the data set from *six-dimensions to two-dimensions* so that data could be visualized directly (see Supporting Information).

### <Figure 3>

*Classification Study.* For classifying and discriminating between the seven odor conditions, only the averaged bead response profiles (as shown in **Figure 2**) and data obtained from repeated observations were used. Both Multivariate Analysis of Variance (MANOVA) and Discriminant Function Analysis (DFA) were used for this purpose. MANOVA was applied to this data-set in order to assess the effect that odor class had on determining the sensor responses, and therefore indicated the likely discriminability of the entire data set. Furthermore, the Wilks's Lambda measure, which indicates the amount of variance not explained by class difference, was used to quantitatively assess the separation of the data for each odor class. Before MANOVA was applied, the underlying assumptions made by the technique: a) multivariate normality, b) homogeneity of the covariance matrix, and c) independence of observations were tested satisfactorily (see Supporting Information).

The MANOVA procedure was applied to each of the pre-processing types, and the results indicated that in each case, a very large effect was present between bead response profiles and odor types (Supporting Information). The best performance was achieved by the array normalized fractional grayscale values corresponding to  $p < 10^{-3}$  and a Wilks's Lambda value of  $1.08 \times 10^{-7}$ . This pre-processing metric was therefore selected for odor type classification using DFA to optimize discrimination performance. The array normalized grayscale values were screened using the Box and Whisker plot and showed no values existed outside of the  $\pm 3$  SD limit indicating the absence of deviant data points (Supporting Information).

While the MANOVA results suggest good class separation for all of the pre-processing metrics, canonical DFA analysis was used to construct a set of linear discriminant functions which could be applied as a transformation on the data values to maximally separate the odor categories (Supporting Information). Only the first two out of six discriminant functions were required to adequately classify the seven odor classes (**Figure 4A**). All five observations for each odor category separate after transformation by the first two discriminant functions. Prescriptive DFA was then performed using the discriminant functions to classify each of the 35 observations into one of seven odor categories. As shown by the confusion matrix in **Table 3**, each observation was classified correctly, as indicated by no off-diagonal terms. A classification rate of 100% was achieved for all seven odor observations at their maximum relative concentration levels.

<**Figure 4**>

<**Table 3**>

In order to obtain an indication of the array's detection limit to each of the three pure and three complex odors, the DFA analysis was repeated using the array normalized fractional values, to also include the lower analyte dilutions for the six odor types (**Table 2**). The challenge was to correctly classify both the maximum concentration observations as well as the reduced concentration observations into their correct odor categories. The DFA results for the six discriminant functions are shown in Supporting Information. A plot of the transformed pre-processed values is shown in **Figure 4B**. As in the first classification task, those observations at maximum concentration were shown to effectively separate in DFA space. The results for the diluted observations, however, were not as well separated and, as expected, were harder to discriminate and classify into odor categories. By applying the same discriminant functions to classify each observation, it was possible to achieve 86.2% correct classification over all concentrations. **Table 4** shows the confusion matrix for this classification. All the values with '1' (b1, c1, d1, e1, g1) represent the analytes at their lowest concentration, those with '2' (b2, d2, g2) represent the second lowest concentration, followed by '3', etc. Most importantly, **Table 4** indicates which of the reduced concentration observations failed to be classified correctly. In all cases, it was the lowest concentration observations that failed to classify correctly, thus indicating the detection limit for this particular array to these analytes. By ignoring the lowest

concentration level for each odor, 93.2% classification is achieved and if the three lowest concentration levels of each odor are ignored, the system classifies all remaining odor observations correctly.

<Table 4>

## CONCLUSIONS

A fiber optic, bead sensor array that can accurately discriminate between six analytes at various dilutions has been described. Discrimination of two VOCs, one NAC, and three coffee bean odors with 100% correct classification was achieved at the highest relative concentration levels (within the data set) and the system was also capable of achieving discrimination at various dilutions. The six sensor materials employed in our study were not pre-selected in any fashion as being particularly good transducers for any of the six odor types, including three types of coffee beans, and air. The sensors were able to fully discriminate all analytes without any sensor-analyte optimizations. This study complements our previous bead-based vapor detection efforts which mainly focused on two-class problems for detecting the presence/absence of specific vapor targets.<sup>14-16</sup> In terms of comparison with other electronic noses, we clearly demonstrate that bead-based sensors can discriminate complex odors, which brings our technology in line with other sensor technologies and proves that it is a viable approach for complex odor discrimination. With the given speed of the fluorescence-based system (faster than other documented nose chemosensors), there is the chance that near-continuous real-time monitoring could take place for industrial process control, as well as food monitoring or smoke detection. The sensors show good reversibility, speed, and diversity to a broad range of organic compounds, making them ideal for both odor classification and individual component concentration prediction tasks. The reproducibility of sensor types has been quantified, as have the relative detection limits to the battery of compounds tested. The properties of this system are also ideal for modeling the olfactory system<sup>32</sup> and can be used to improve on any practical applications of this array platform, that is, the ability to produce multiple sensor arrays with transferable computational classifiers.<sup>16</sup>

## ACKNOWLEDGEMENTS

The Tufts work is supported by the Defense Advanced Research Projects Agency and the Office of Naval Research and the Leicester work is funded by the Royal Society, London.

## REFERENCES

- (1) Persaud, K. C.; Dodd, G. H. *Nature* **1982**, *299*, 352-355.
- (2) Carey, W. P.; Beebe, K. R.; Kowalski, B. R. *Anal. Chem.* **1987**, *57*, 1529-1534.
- (3) Gardner, J. W.; Bartlett, P. N. *Electronic Noses: Principles and Applications*; Oxford University Press: Oxford, UK, 1999.
- (4) Lonergan, M. C.; Severin, E. J.; Doleman, B. J.; Beaver, S. A.; Grubbs, R. H.; Lewis, N. S. *Chem. Mater.* **1996**, *8*, 2298-2312.
- (5) Stetter, J. R.; Jurs, P. C.; Rose, S. L. *Anal. Chem.* **1986**, *58*, 860-866.
- (6) Albert, K. J.; Lewis, N. S.; Schauer, C. L.; Sotzing, G. A.; Stitzel, S. E.; Vaid, T. P.; Walt, D. R. *Chem. Rev.* **2000**, *100*, 2595-2626.
- (7) Jurs, P. C.; Bakken, G. A.; McClelland, H. E. *Chem. Rev.* **2000**, *100*, 2649-2678.
- (8) Gardner, J. W. *Sens. Actuators B* **1992**, *4*, 109-115.
- (9) Shaffer, R. E.; Rose-Pehrsson, S. L.; McGill, R. A. *Analytical Chimica Acta* **1999**, *384*, 305-317.
- (10) Hines, E. L.; Llobet, E.; Gardner, J. W. *IEE Proceedings-Circuits Devices and Systems* **1999**, *146*, 297-310.
- (11) Sicard, G.; Holley, A. *Brain Research* **1984**, *292*, 283-296.
- (12) Rouhi, M. *Chemical and Engineering News* **1999**, *75*, 29-March, 58.
- (13) Albert, K. J.; Walt, D. R. *Anal. Chem.* **2000**, *72*, 1947-1955.
- (14) Bakken, G. A.; Kauffman, G. W.; Jurs, P. C.; Albert, K. J.; Stitzel, S. E. *in press*.
- (15) Albert, K. J.; Myrick, M. L.; Brown, S. B.; James, D. L.; Milanovich, F.; Walt, D. R. , *in press*.
- (16) Stitzel, S. E.; Cowen, L.; Albert, K. J.; Walt, D. R. , *manuscript submitted*.
- (17) Clarke, R. J.; Macrae, R.; Eds. *Coffee, Vol. 1: Chemistry*; Elsevier Applied Science Publishers: New York, 1985.
- (18) Legin, A.; Rudnitskaya, A.; Vlasov, Y.; Di Natale, C.; Davide, F.; D'Amico, A. *Sens. Actuators B* **1997**, *44*, 291-296.
- (19) Singh, S.; Hines, E. L.; Gardner, J. W. *Sens. Actuators B* **1996**, *30*, 185-190.
- (20) Gardner, J. W.; Shurmer, H. V.; Tan, T. T. *Sens. Actuators B* **1992**, *6*, 71-75.
- (21) Llobet, E.; Hines, E. L.; Gardner, J. W.; Bartlett, P. N.; Mottram, T. T. *Sens. Actuators B* **1999**, *61*, 183-190.
- (22) Ulmer, H.; Mitrovics, J.; Noetzel, G.; Weimar, U.; Gopel, W. *Sens. Actuators B* **1997**, *43*, 24-33.
- (23) Dickinson, T. A.; White, J.; Kauer, J. S.; Walt, D. R. *Nature* **1996**, *382*, 697-700.
- (24) White, J.; Kauer, J. S.; Dickinson, T. A.; Walt, D. R. *Anal. Chem.* **1996**, *68*, 2191-2202.

- (25) Pantano, P.; Walt, D. R. *Analytical Chemistry* **1995**, *67*, A481-A487.
- (26) Pantano, P.; Walt, D. R. *Chemistry of Materials* **1996**, *8*, 2832-2835.
- (27) Michael, K. L.; Taylor, L. C.; Shultz, S. L.; Walt, D. R. *Anal. Chem.* **1998**, *70*, 1242-1248.
- (28) Vauthey, E. *Chemical Physics Letters* **1993**, *216*, 530-536.
- (29) Meinershagen, J. L.; Bein, T. *J. Am. Chem. Soc.* **1999**, *121*, 448-449.
- (30) Deye, J. F.; Berger, T. A. *Anal. Chem.* **1990**, *62*, 615-622.
- (31) Dickinson, T. A.; Michael, K. M.; Kauer, J. S.; Walt, D. R. *Anal. Chem.* **1999**, *71*, 2192-2198.
- (32) Pearce, T. C.; Verschure, P. F. M. J. V.; White, J.; Kauer, J. S. *Neurocomputing* **2000**, *in press*.
- (33) Kauer, J. S.; Shepherd, G. J. *Physiol.* **1977**, *272*, 495-516.
- (34) Howard, P. H.; Meylan, W. M. *Handbook of Physical Properties of Organic Chemicals*; Lewis Publishers: New York, 1997.
- (35) made available for public use at the info-Labview VI archive <ftp://ftp.pica.army.mil/pub/labview/vi/>; .
- (36) Pearce, T. C.; Gardner, J. W. *Analyst* **1998**, *123*, 2057-2066.
- (37) Doleman, B. J.; Severin, E. J.; Lewis, N. S. *Proc. Natl. Acad. Sci. U.S.A.* **1998**, *95*, 5442-5447.

## **Figure Legends**

**Figure 1:** CCD images of each imaging fiber bundle. Bundle *A-C* (top) and bundle *D-F* (bottom) showing the fitted regions of interest (ROIs) corresponding to each addressable bead sensor. A total of 2683 sensors were analyzed: (A) 814 beads; (B) 286 beads; (C) 301 beads; (D) 692 beads; (E) 294 beads; and (F) 296 beads. The ROIs were drawn using Labview<sup>TM</sup> and IMAQ Vision<sup>TM</sup> software. Each imaging fiber's face is 1 mm<sup>2</sup>. Images were acquired with 100 ms exposure time and excitation/emission filters were 560 (bp 40) nm and 630 (bp 20) nm respectively.

**Figure 2:** Average normalized time responses for each bead type during a single test sequence to an odor pulse for each of the odor categories: (a) air (control), (b) toluene, (c) acetone, (d) 1,3-DNB, (e) Hazelnut coffee beans, (f) Columbian coffee beans, and (g) French Roast coffee beans. The color-coding for each bead type matches that used for **Figure 1**: *A* (red); *B* (green); *C* (blue); *D* (magenta); *E* (aqua); and *F* (yellow). The solid black bar indicates the presence and duration of the 1.81 s odor stimulus.

**Figure 3:** Radar plots showing the difference in the average fractional response to the highest concentrations of each odor class (5 repeated runs of each class) for each bead type (*A-F*) to odors (a-f) as listed in **Figure 2**. In each case the dashed lines indicate  $\pm 1$  standard deviation (SD) in the average bead response across the population of sensors analyzed. Positive values indicate an overall increase in grayscale value to the odor while negative values indicate an overall decrease.

**Figure 4:** Results of DFA analysis as applied to the array normalized fractional grayscale pre-processed values. (A) First two discriminant functions for maximum odor concentrations of (a-f) as listed in **Figure 2**. (B) First two discriminant functions for combined maximum and diluted concentrations of the seven odor categories. First letter indicates the odor category and the second number indicates the concentration level, 1 – lowest concentration, 2 – second lowest concentration, etc. No number – highest concentration.

## **Figure Legends**

**Figure 1:** CCD images of each imaging fiber bundle. Bundle *A-C* (top) and bundle *D-F* (bottom) showing the fitted regions of interest (ROIs) corresponding to each addressable bead sensor. A total of 2683 sensors were analyzed: (A) 814 beads; (B) 286 beads; (C) 301 beads; (D) 692 beads; (E) 294 beads; and (F) 296 beads. The ROIs were drawn using Labview<sup>TM</sup> and IMAQ Vision<sup>TM</sup> software. Each imaging fiber's face is 1 mm<sup>2</sup>. Images were acquired with 100 ms exposure time and excitation/emission filters were 560 (bp 40) nm and 630 (bp 20) nm respectively.

**Figure 2:** Average normalized time responses for each bead type during a single test sequence to an odor pulse for each of the odor categories: (a) air (control), (b) toluene, (c) acetone, (d) 1,3-DNB, (e) Hazelnut coffee beans, (f) Columbian coffee beans, and (g) French Roast coffee beans. The color-coding for each bead type matches that used for **Figure 1**: *A* (red); *B* (green); *C* (blue); *D* (magenta); *E* (aqua); and *F* (yellow). The solid black bar indicates the presence and duration of the 1.81 s odor stimulus.

**Figure 3:** Radar plots showing the difference in the average fractional response to the highest concentrations of each odor class (5 repeated runs of each class) for each bead type (*A-F*) to odors (a-f) as listed in **Figure 2**. In each case the dashed lines indicate  $\pm 1$  standard deviation (SD) in the average bead response across the population of sensors analyzed. Positive values indicate an overall increase in grayscale value to the odor while negative values indicate an overall decrease.

**Figure 4:** Results of DFA analysis as applied to the array normalized fractional grayscale pre-processed values. (A) First two discriminant functions for maximum odor concentrations of (a-f) as listed in **Figure 2**. (B) First two discriminant functions for combined maximum and diluted concentrations of the seven odor categories. First letter indicates the odor category and the second number indicates the concentration level, 1 – lowest concentration, 2 – second lowest concentration, etc. No number – highest concentration.

## **List of Tables**

**Table 1.** Microsensor materials employed.

**Table 2.** Sixty five odor observations employed for odor discrimination.

**Table 3:** Confusion matrix produced by applying prescriptive DFA to the array normalized fractional pre-processed grayscale values obtained from thirty five observations at maximum concentration. The average classification rate is 100%.

**Table 4:** Confusion matrix produced by applying prescriptive DFA to the array normalized fractional pre-processed grayscale values obtained from thirty five samples at maximum concentrations and thirty samples at diluted concentration. Average classification rate 86.2%.

## **Supporting Information Section**

**Figure SI-1:** Principal Components Analysis plots obtained for the fractional grayscale metric for the highest concentrations of each odor class (5 repeated runs of each class). (A) A screen plot of the eigenvalues for the covariance matrix and (B) a plot of the first two principal components for each odor observation (a-f) as listed in **Figure 2**.

**Figure SI-2:** Box & Whisker Plot for the array normalized fractional grayscale response for each of the six bead types to each of the seven odor categories. There are *no* values outside of  $\pm 3$  SD shown for either category indicating that no outliers exist.

**Table SI-1:** Details for the PCA analysis carried out on the fractional grayscale pre-processed values.

**Table SI-2:** Results of MANOVA as applied to the classification problem. A – array normalized, S – sensor autoscaled, N- no normalization, F – fractional metric, R- relative metric, D – difference metric. †significance level too small to calculate.

**Table SI-3:** Details for the DFA analysis carried out on the array normalized fractional pre-processed values for the observations at maximum concentration levels. †significance level too small to calculate.

**Table SI-4:** Details for the DFA analysis carried out on the array normalized fractional pre-processed values for the combined maximum and diluted concentration samples. †significance level too small to calculate.

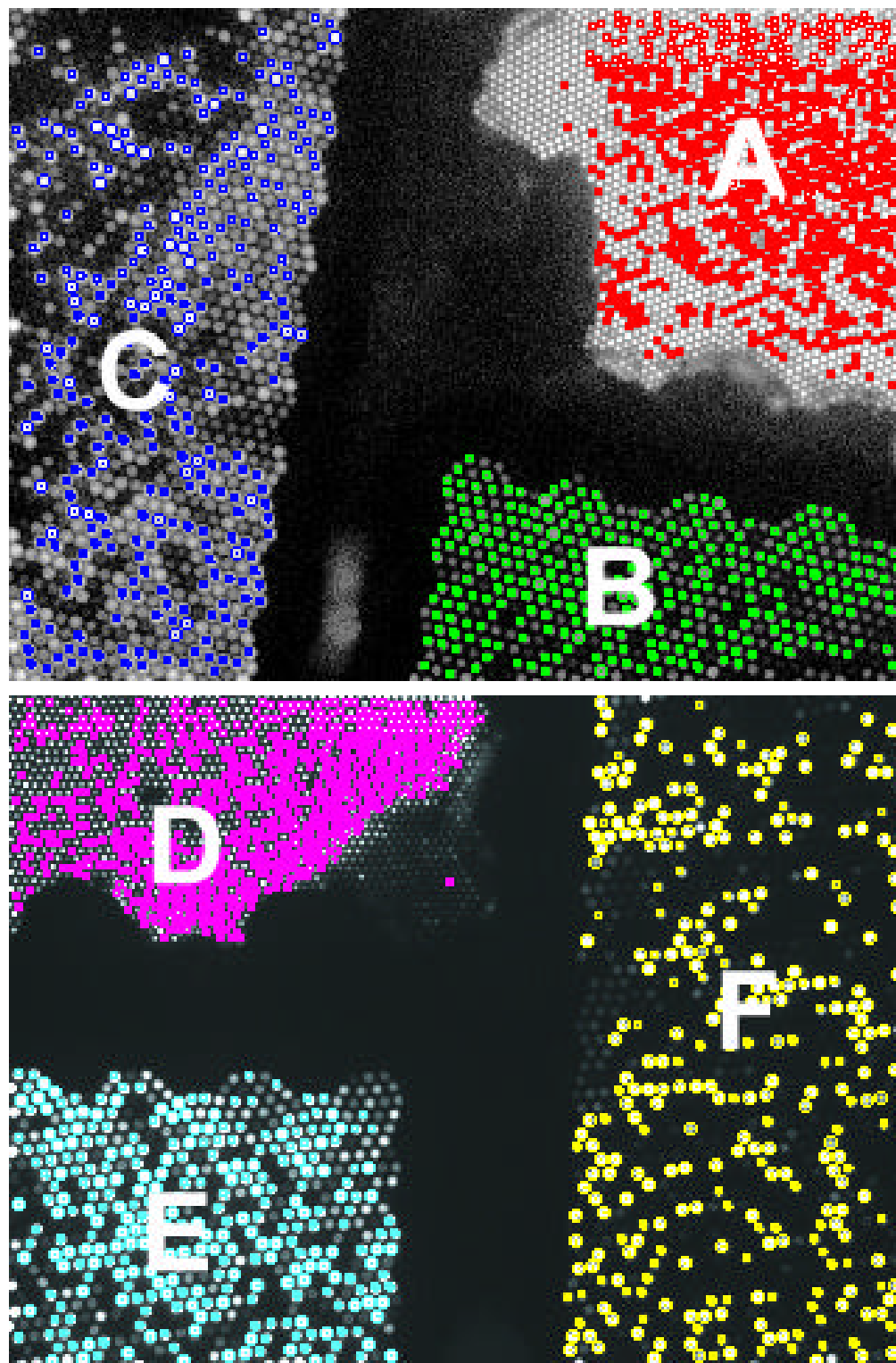


Figure 1.

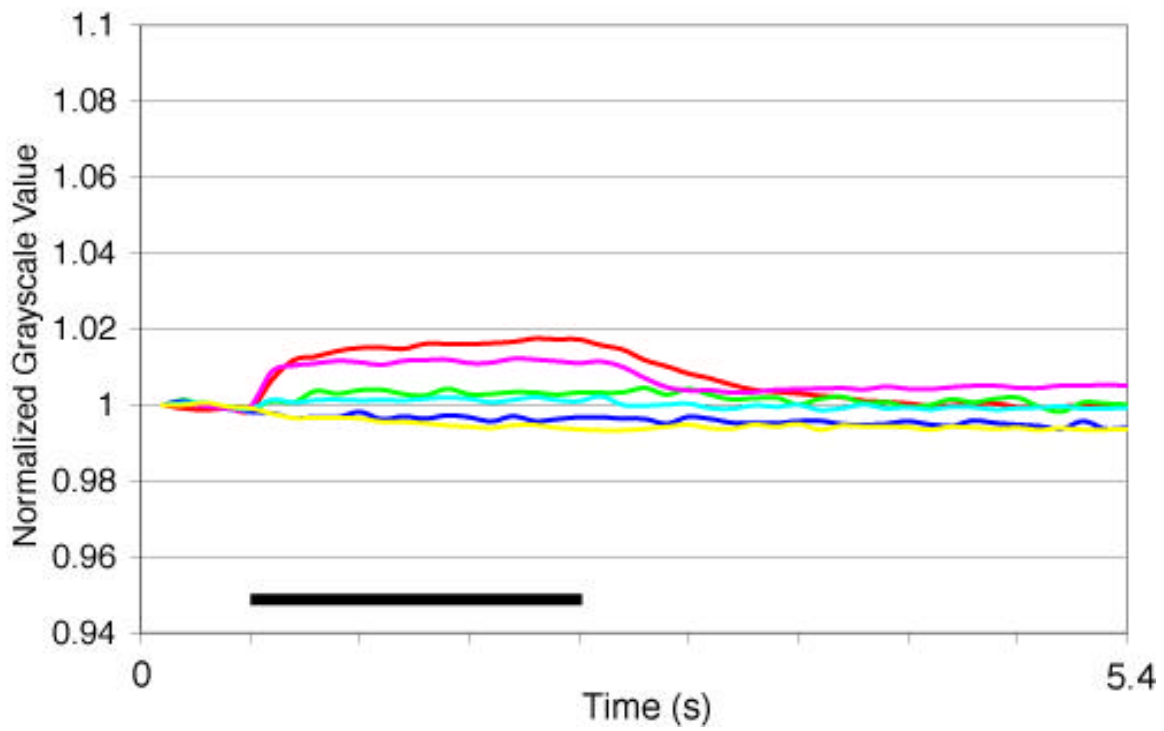


Figure 2a

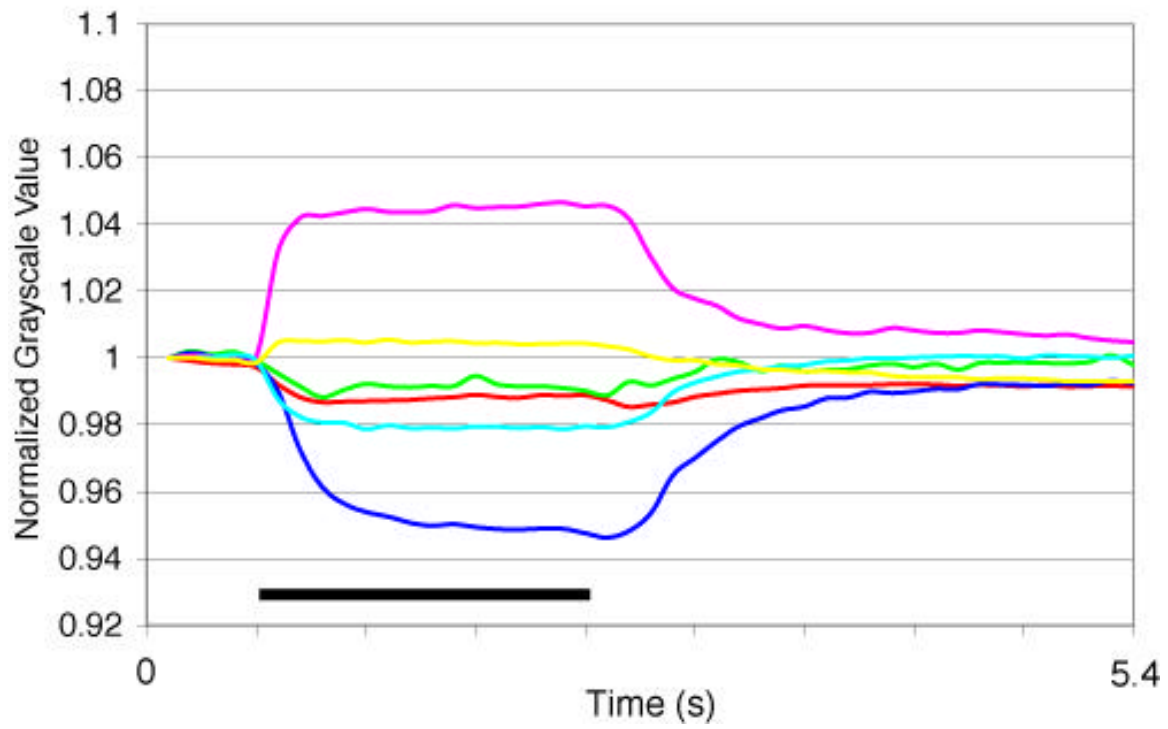


Figure 2b

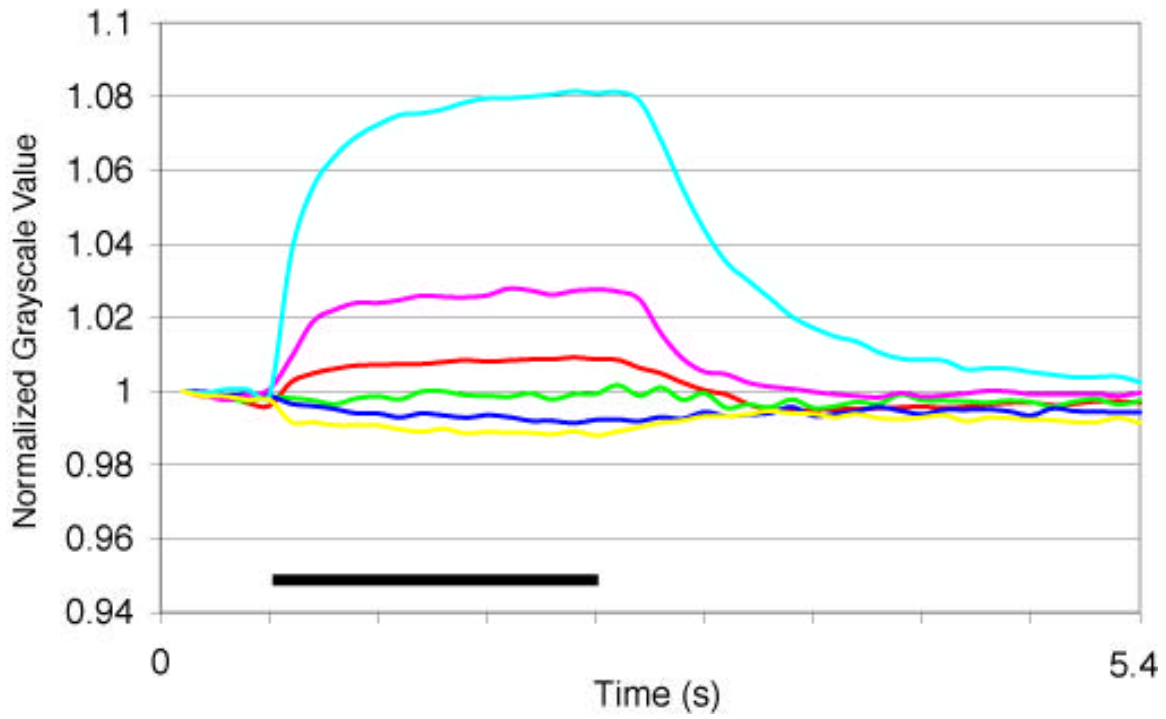


Figure 2c

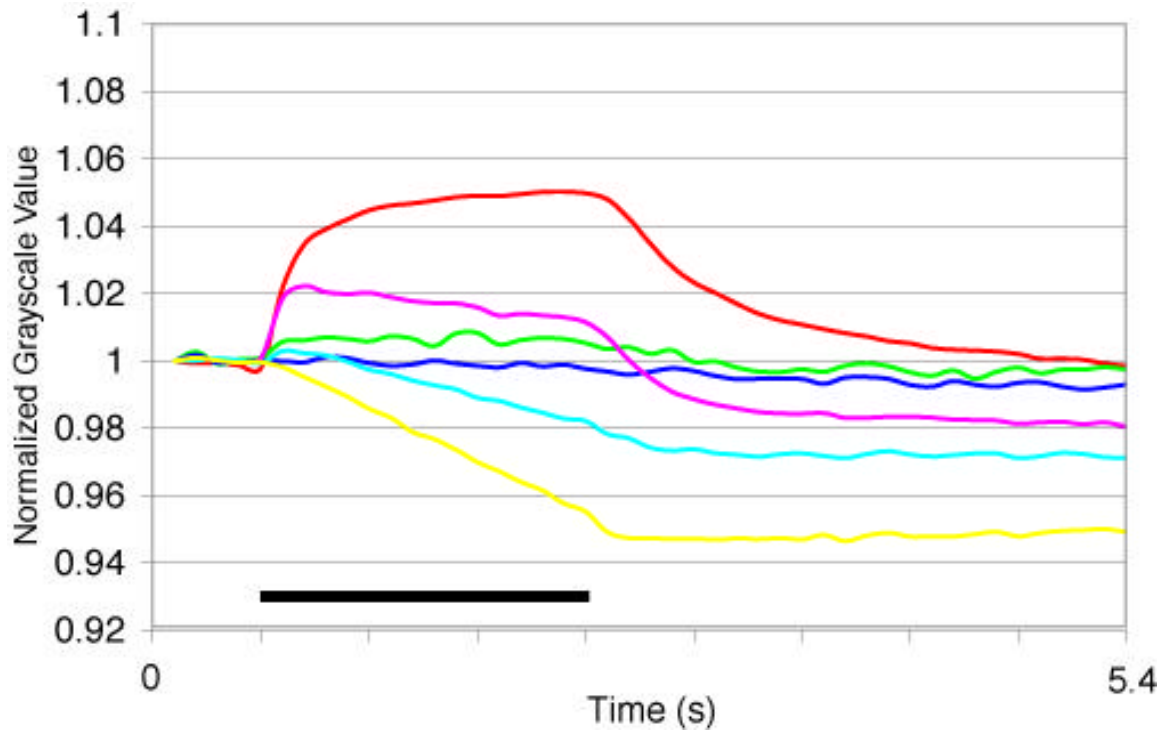


Figure 2d

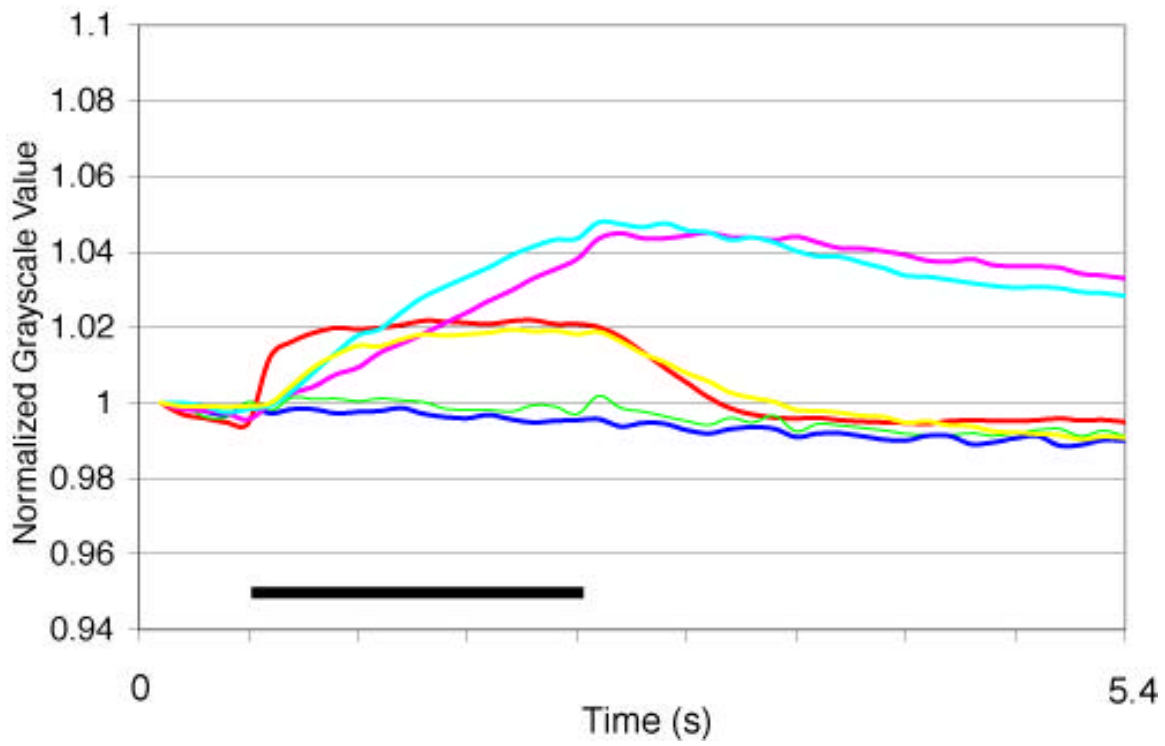


Figure 2e

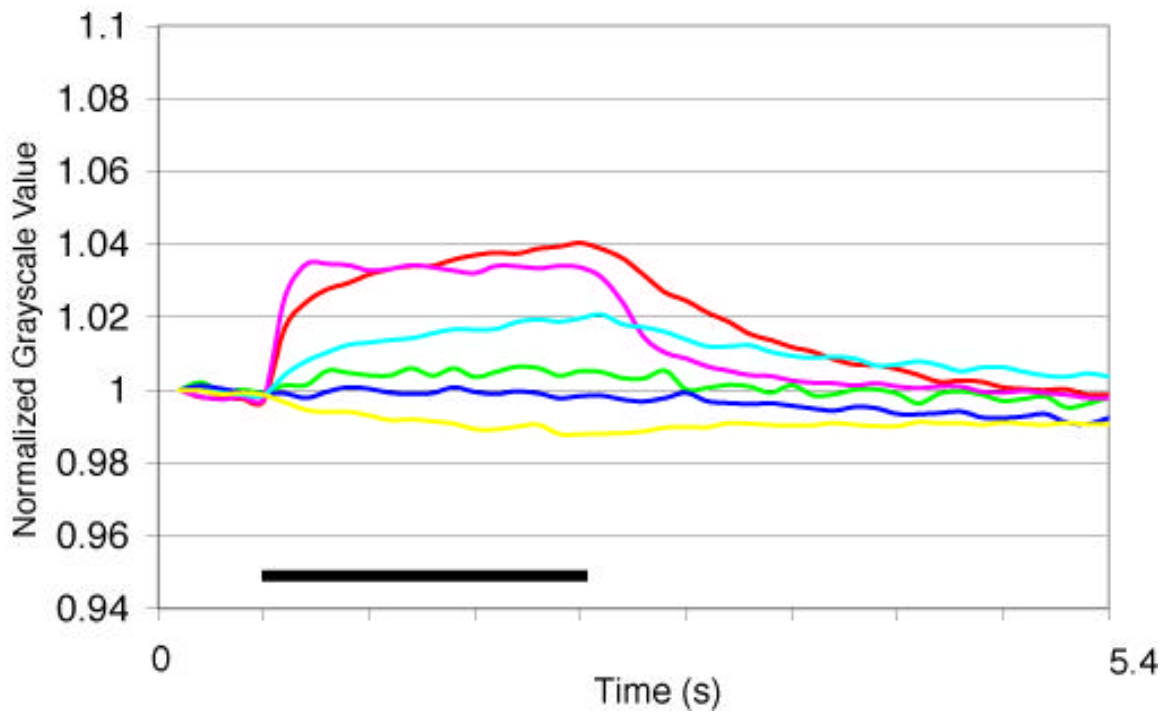
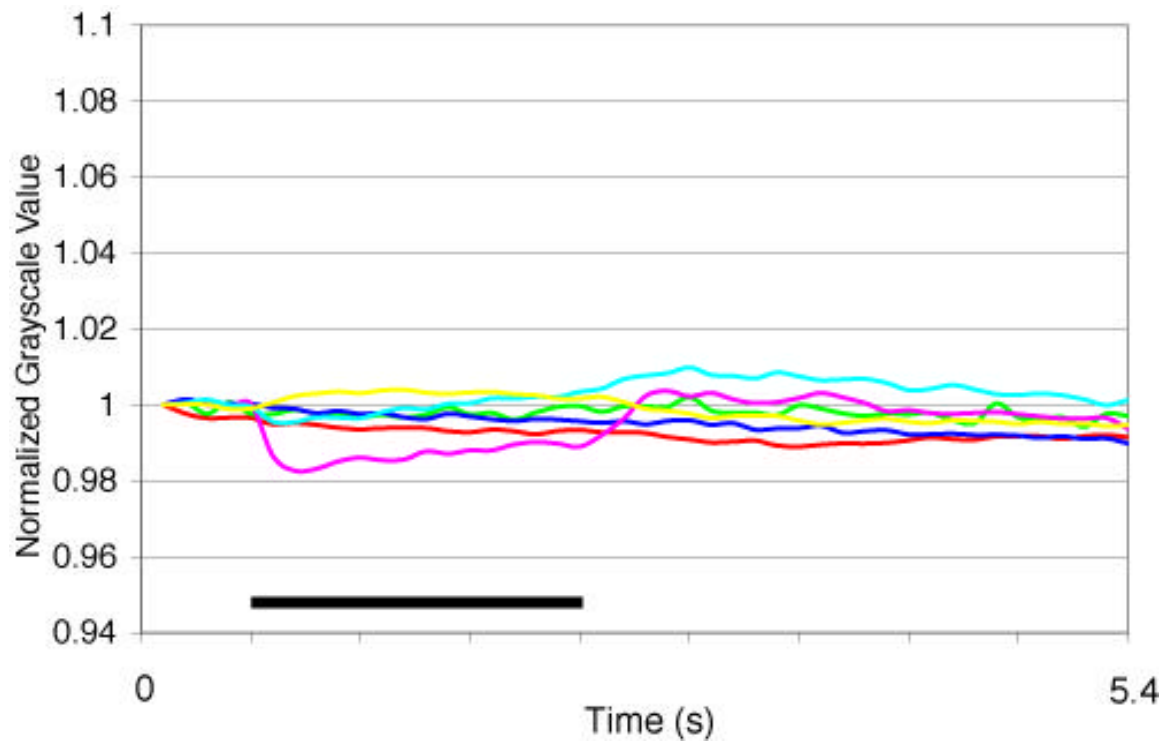


Figure 2f



**Figure 2g**

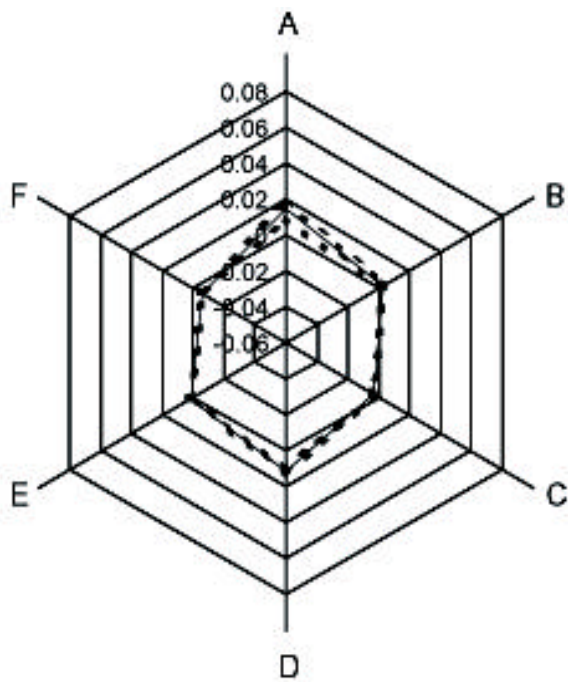


Figure 3a

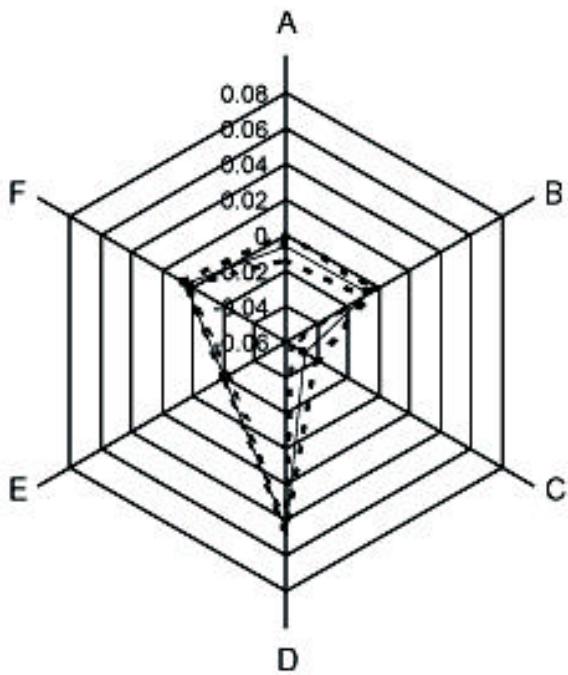


Figure 3b

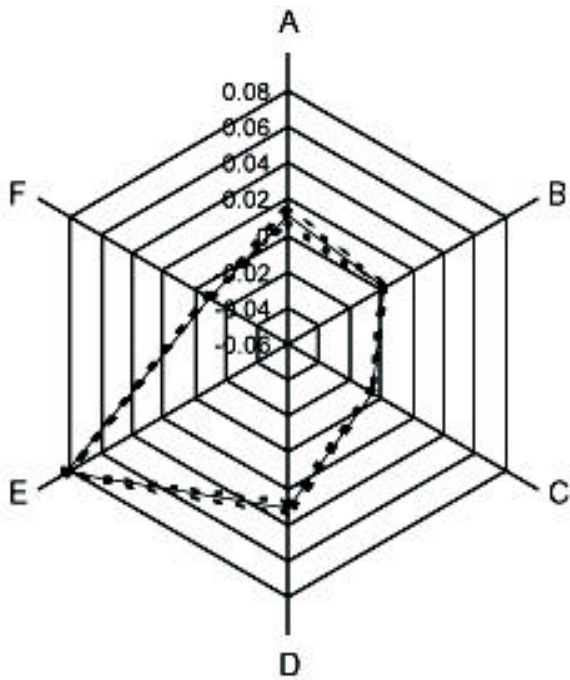


Figure 3c

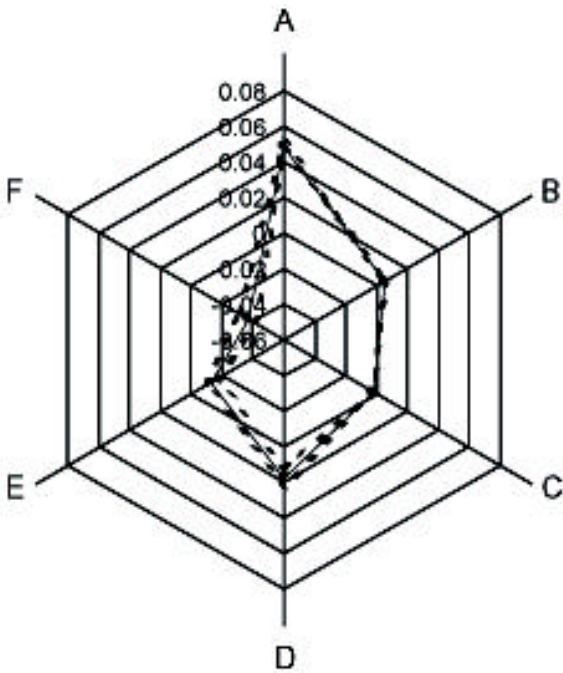


Figure 3d

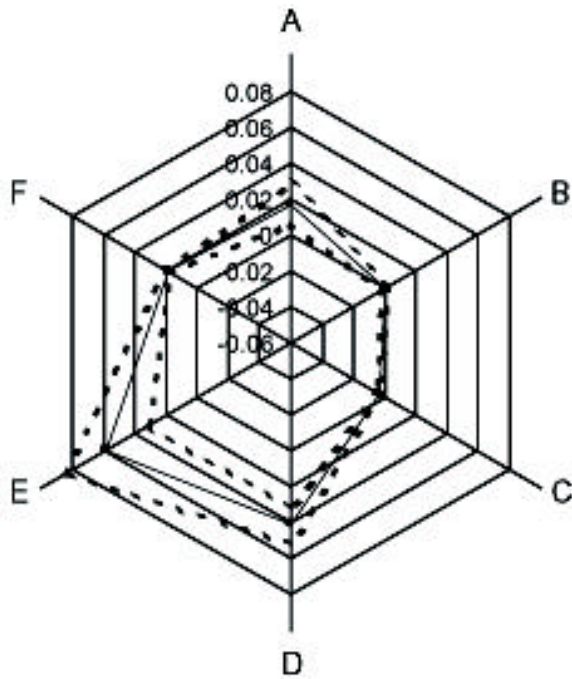


Figure 3e

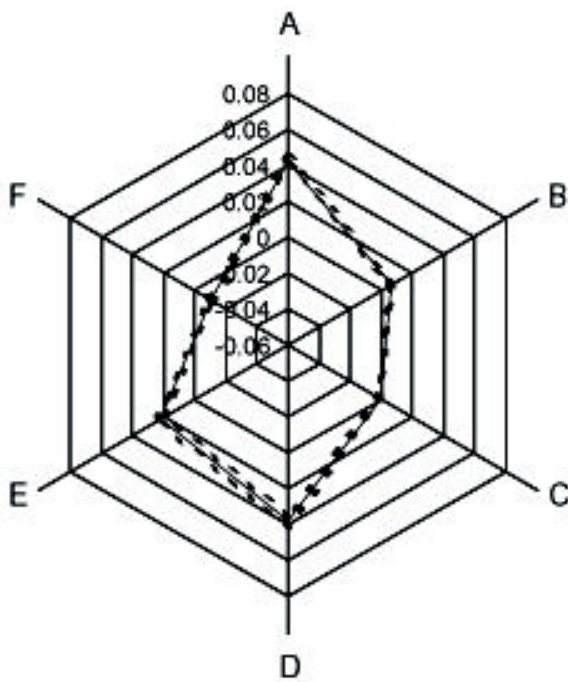


Figure 3f

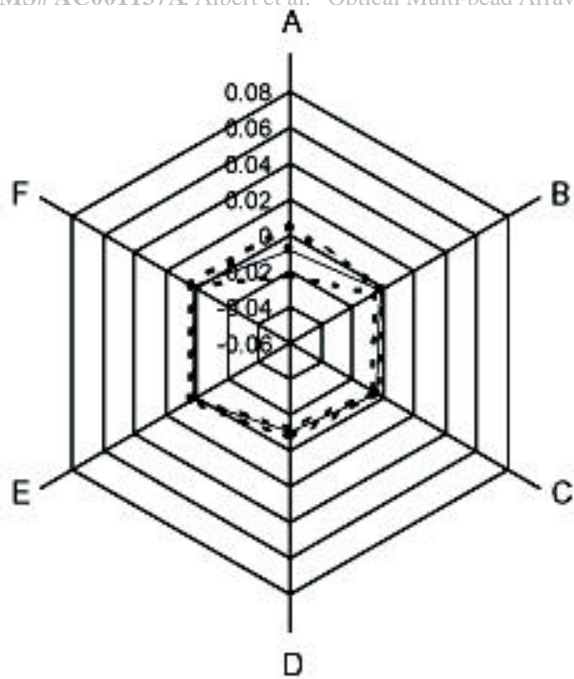


Figure 3g

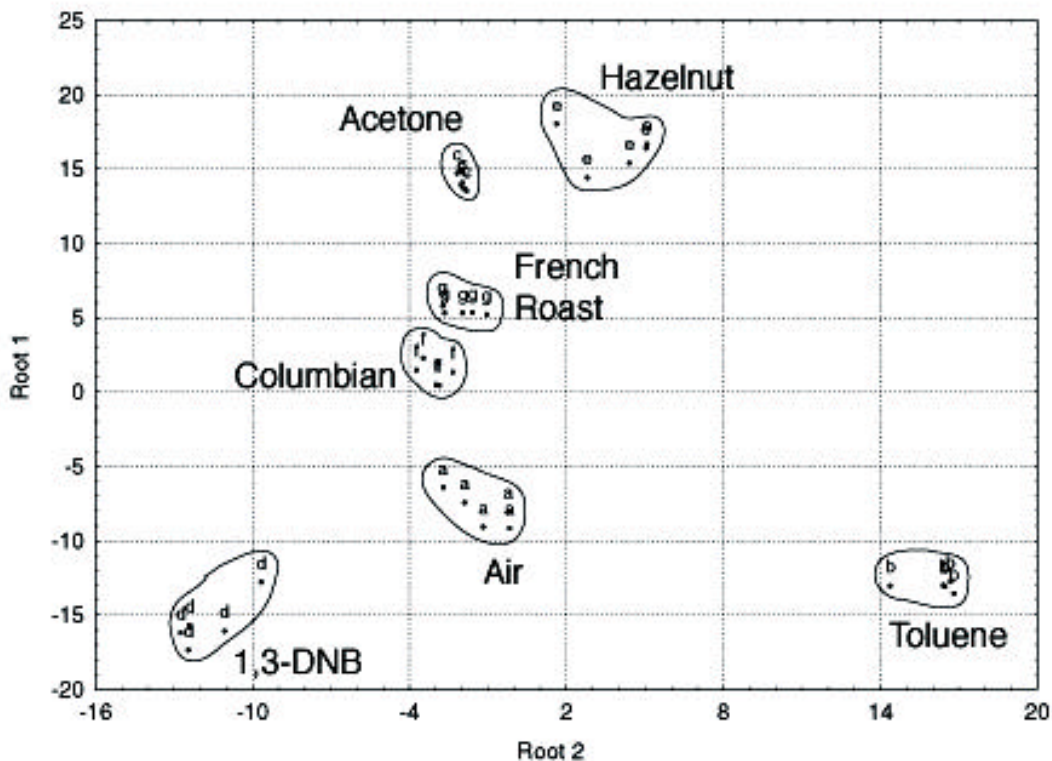


Figure 4a

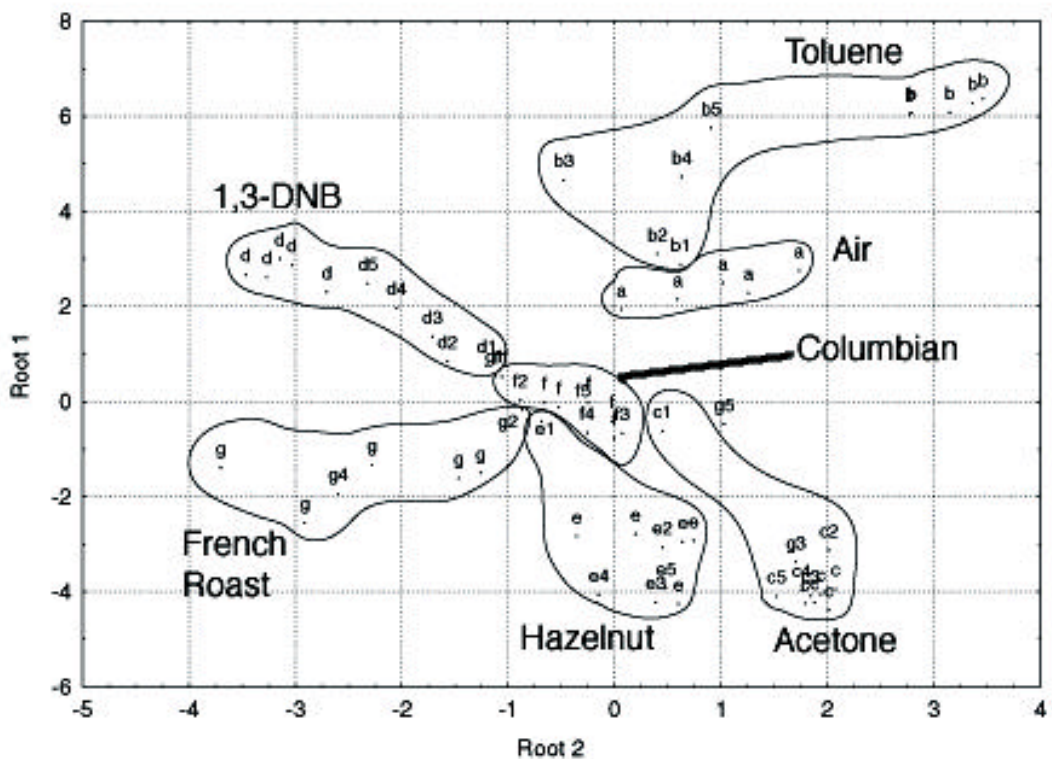


Figure 4b

**Table 1. Microsensor materials employed**

<b>Sensor Name</b>	<b>Size (mm)</b>	<b>Microsphere Material<sup>a</sup></b>	<b>Surface Modification<sup>b</sup></b>	<b>Pore Size (Å)</b>	<b>No. Sensors Analyzed</b>
<b>A</b>	5	Chirex	3012 <sup>c</sup>	not known	814
<b>B</b>	5	Spherex	aniline	100	286
<b>C</b>	3	Phenosphere	cyano (-CN)	80	301
<b>D</b>	3	Phenosphere	hydroxy (-OH)	80	692
<b>E</b>	5	Develosil	hydroxyl (-OH)	60	294
<b>F</b>	5	Phenosphere	cyano (-CN)	80	296

<sup>a</sup>materials are named according to the distributor (Phenomenex, Torrance, CA)

<sup>b</sup>materials were either purchased or modified with particular surface functionalities. All sensors were stained with Nile Red dye and stored dry, except sensor type **C**, which was stored in 0.01% Tween/DI Water (see experimental).

<sup>c</sup>(R)-phenylglycine and 3,5-dinitroaniline urea linkage

**Table 2. Odor Observations (ppm)<sup>a</sup>**

<u>Air</u>	<u>Acetone</u>	<u>Toluene</u>	<u>1,3-DNB</u>	<u>Three Coffee Types</u>
(blank)	450	450	0.1	10%
	1800	1800	0.2	20%
	3600	3600	0.4	40%
	5400	5400	0.6	60%
	7200	7200	0.8	80%
	9000	9000	0.9	90%

<sup>a</sup>all exposures are in ppm, except the three coffee types, which were done as percent saturated, i.e., 90% saturation involves 10% air dilution. The highest concentration for each odor was repeated five times.

**Table 3**

		PREDICTED CLASS						
		Air	Toluene	Acetone	DNB	Hazulnut coffee	Columbian coffee	French Roast coffee
A C T U A L  C L A S S	Air	5	0	0	0	0	0	0
	Toluene	0	5	0	0	0	0	0
	Acetone	0	0	5	0	0	0	0
	DNB	0	0	0	5	0	0	0
	Hazulnut coffee	0	0	0	0	5	0	0
	Columbian coffee	0	0	0	0	0	5	0
	French Roast coffee	0	0	0	0	0	0	5

**Table 4**

		PREDICTED CLASS						
		Air (a)	Toluene (b)	Acetone (c)	DNB (d)	Hazulnut coffee (e)	Columbian coffee (f)	French Roast coffee (g)
A C T U A L  C L A S S	Air (a)	5	0	0	0	0	0	0
	Toluene (b)	2 (b1, b2)	8	0	0	0	0	0
	Acetone (c)	0	0	9	0	0	1 (c1)	0
	DNB (d)	0	0	0	8	0	2 (d1, d2)	0
	Hazulnut coffee (e)	0	0	0	0	9	1 (e1)	0
	Columbian coffee (f)	0	0	0	0	0	10	0
	French Roast coffee (g)	0	0	1 (g3)	0	0	2 (g1, g2)	7

## Supporting Information

### Optical Multi-bead Arrays for Simple and Complex Odor Discrimination

**Keith J. Albert and David R. Walt\***

The Max Tishler Laboratory for Organic Chemistry, Department of Chemistry, Tufts University, Medford, MA 02155 \*Corresponding author for sensor work. Fax: 617.627.3443; Email: [david.walt@tufts.edu](mailto:david.walt@tufts.edu)

**Daljeet S. Gill and Tim C. Pearce\***

Department of Engineering, University of Leicester, Leicester LE1 7RH, United Kingdom \*Corresponding author for computational work. Tele: +44(0)116.223.1290 Fax: +44(0)116.252.2619; Email: [t.c.pearce@leicester.ac.uk](mailto:t.c.pearce@leicester.ac.uk)

The supporting information section is eight pages (including the cover sheet).

Two figures (**Figure SI-1 & SI-2**), four tables (**Tables SI-1, SI-2, SI-3, & SI-4**) and a reference section are included in the Supporting Information section. The tables and figure legends for Supporting Information are at the end of this document.

## Supporting Information

This section gives a detailed description of the statistical techniques used for data analysis that were not included in the main report.

### EXPERIMENTAL SECTION

*Sensor B fabrication.* The aniline functionalized beads (*B*) were prepared by placing 50 mg Spherex (-OH) packing material into a glass vial with 1 mL 10% (v/v) N-[3-(trimethoxysilyl)propyl]aniline in acetone. The beads were shaken vigorously on a vortexer for two hours, rinsed with copious amounts of ethanol, and centrifuged for 40 s at 4000 rpm. The solution was decanted, ethanol was added, and the beads were vortexed and centrifuged. This process was repeated three times to wash the beads of excess silane solution. The beads were then placed in an oven for 30 min at 110°C and then rinsed with toluene, vortexed, centrifuged, and the solution was decanted (repeated three times). The beads were added to 1 mL 0.5 mg/mL Nile Red/Toluene solution and vortexed 3 hrs. The beads were centrifuged with successive rinsing steps with toluene, DI water, and ethanol. All stained microsphere sensors (*A-F*) were placed in individual 4 mL glass vials, dried in an oven (110°C) for 1 hr, and then stored in the dark at room temperature until use.

*Tedlar bag sample preparation.* Precise control of flow rates was accomplished by rotometers (Fisher) and proper filling time was calculated according to the required analyte concentration. The volume of solvent added to 30 L carrier air to produce 10,000 ppm analyte vapor in the bags, were 0.985 mL and 1.423 mL for acetone and toluene respectively. Once prepared, the 10,000 ppm tedlar-bag analyte samples were allowed to equilibrate overnight at room temperature to ensure uniform odor distribution.

### RESULTS & DISCUSSION

Principal Components Analysis (PCA), carried out before the classification study, was used as the standard technique to reduce the dimensionality of the data set from *six-dimensions to two-dimensions* so that the data could be visualized directly. We applied the generally accepted rule<sup>1</sup> that the subjects-to-variables (STV) ratio must be at least 5 in order to apply PCA – in this case a total of thirty five maximum concentration observations (subjects) to six bead types (variables). Since PCA relies upon extracting the eigenvalues of the covariance matrix for

## Supporting Information

the data, it was necessary to consider how well conditioned the eigensystem was by plotting the eigenvalues in rank order (sometimes referred to as a scree plot) as shown for the fractional grayscale preprocessed values in Figure SI-1A. Clearly the rank ordered eigenvalues show a well conditioned monotonically decreasing relationship, confirming the suitability of PCA for this data-set. Different stopping rules may be employed to judge how many factors may be reasonably extracted using PCA. We have used Kaiser's "stopping rules" which permits the extraction of principal components until the corresponding eigenvalue is less than one.<sup>2</sup> This extraction is reasonable since PCA was employed as a dimensionality reduction technique, so factors with corresponding eigenvalues below one contribute less to the total variance than the average sensor and can be ignored. Using Kaiser's stopping rule it was clear that a maximum of three principal components could be extracted. For purposes of clarity, Figure SI-1B shows the transformed data for only the first two principal components, as applied to the fractional grayscale metric, and describes a large portion of the total variance (72.4%). Figure SI-1B shows reasonable odor class separation although there is clearly some overlap between the transformed data for acetone and Hazelnut coffee. The overlap between these two classes was also evident for all PCA plots for each type of pre-processing metric (not shown). Even using this relatively simple unsupervised classification method, five of the seven odor classes may be easily discriminated. For the remaining classes, full discrimination would be possible (at the highest concentration level) by using the averaged time-dependent response profiles for the five repeated observations in each case. Table SI-1 shows the details for each extracted principal component. By considering the factor loadings it is possible to assess each bead type's contribution to each principal component. For the fractional pre-processed values, it is clear that all six bead types contribute to the variance described by the first two components. The factor loadings, however, give no indication for each individual sensor's ability to contribute to the prediction results.

<Table SI-1>

<Figure SI-1>

*Classification Study.* Both Multivariate Analysis of Variance (MANOVA) and Discriminant Function Analysis (DFA) were used for classifying and discriminating between the

## Supporting Information

seven odor conditions. Before MANOVA was applied, however, it was necessary to test the underlying assumptions made by the technique: a) multivariate normality, b) homogeneity of the covariance matrix, and c) independence of observations. Multivariate normality was checked by plotting an array of 6 × 6 scatter plots for each bead type's fractional responses against the fractional responses for every other bead type (not shown). An insufficient number of observations were available to accurately verify if each bead type's response data were normally distributed, even though none of the distributions clearly violated this condition. The sensor responses were clearly linearly related in the multivariate scatterplots, i.e. non-linear dependencies between sensor responses were not evident, and this relationship satisfies a further requirement of multivariate normality within the data-set as a whole. Homogeneity of the covariance matrix was checked using the Brown-Forthsythe Test. There were almost no significant differences between the within-group covariance groups within each odor class. This test was fairly homogenous showing reasonable conformance with the second assumption for MANOVA. Independence of observations was ensured by allowing sufficient time to elapse between analyte exposures which gave the sensors time to recover to their original (baseline) values. This process also minimized interference between each of the odor observations.

The MANOVA procedure was applied to each of the pre-processing types, and the results indicated a very large effect was present between bead response profiles and odor types (**Table SI-2**). The Wilks's Lambda values indicate that nearly all the data variance is accounted for by odor category, indicating good discriminability in the data set. Furthermore, the very low *p*-values provide assurance that this effect was highly statistically significant with very little chance of making a Type 1 error. The best performance was achieved by the array normalized fractional grayscale values and was therefore selected for odor type classification using DFA to optimize discrimination performance. In addition to the assumptions made by MANOVA regarding the observation data, DFA is known to be very sensitive to the presence of outliers within a data-set, so the array normalized grayscale values were first screened using a number of methods. Of these methods, the Box and Whisker plot (**Figure SI-2**) shows that no outliers existed, e.g., no values exist outside of ±3 SD limit indicating the absence of deviant data points.

<Table SI-2>

## Supporting Information

### <Figure SI-2>

Canonical DFA analysis was used to construct a set of linear discriminant functions which could be applied as a transformation on the data values to maximally separate the odor categories. The DFA results on the selected array normalized fractional grayscale values for eigenvalue, percent contribution, and significance level for each discriminant function ( $a_i$ ) are shown in **Table SI-3**. Because seven odor classes existed, only six discriminant functions were constructed. The values for the sixth discriminant function ( $a_6$ ), however, were too small to be calculated. The eigenvalues indicated the relative importance for each discriminant function for describing odor class differences. In order to extract a significance level for each of the discriminant functions, a  $\chi^2$  test was performed. Each significance level, except for  $a_5$ , was below 0.05 and was therefore considered reliable (**Table SI-3**). In fact, only the first two discriminant functions were required to adequately classify the seven odor classes and all five observations for each odor category separate after transformation. Prescriptive DFA was then performed using the discriminant functions to classify each of the 35 observations into one of seven odor categories. A classification rate of 100% was achieved for all seven odor observations at their maximum relative concentration levels.

### <Table SI-3>

In order to obtain an indication of the array's detection limit, lower analyte dilutions for the six odor types were included. The DFA analysis was repeated using the array normalized fractional values. The DFA results for the first six discriminant functions are shown in **Table SI-4**. Again, the  $p$ -values strongly show significant results because only one value is  $> 0.05$ . Observations at maximum concentration were shown to effectively separate in DFA space. The results for the diluted observations, however, were harder to discriminate and classify into odor categories. By applying the same discriminant functions to classify each observation, it was possible to achieve 86.2% correct classification over all concentrations.

### <Table SI-4>

## Supporting Information

### Figure legends & table descriptions for Supporting Information (SI) section:

**Figure SI-1:** Principal Components Analysis plots obtained for the fractional grayscale metric for the highest concentrations of each odor class (5 repeated runs of each class). (A) A screen plot of the eigenvalues for the covariance matrix and (B) a plot of the first two principal components for each odor observation (a-f) as listed in **Figure 2**.

**Figure SI-2:** Box & Whisker Plot for the array normalized fractional grayscale response for each of the six bead types to each of the seven odor categories. There are *no* values outside of  $\pm 3$  SD shown for either category indicating that no outliers exist.

**Table SI-1:** Details for the PCA analysis carried out on the fractional grayscale pre-processed values.

Principal Component No.	Variance	Cumulative Variance	Variance (%)	Cumulative Variance (%)	Sensors Contributing
1	2.884	2.884	48.1	48.1	A, B, C, F
2	1.460	4.344	24.3	72.4	D, E, F
3	1.163	5.507	19.4	91.8	A, C, E
4	0.396	5.903	6.6	98.4	E, F
5	0.062	5.965	1.0	99.4	A, B, C
6	0.035	6.000	0.6	100.0	-

## Supporting Information

**Table SI-2:** Results of MANOVA as applied to the classification problem. A – array normalized, S – sensor autoscaled, N- no normalization, F – fractional metric, R- relative metric, D – difference metric.

Preprocessing Metric	Normalization	Wilks's Lambda	<i>p</i> -value
F	N	$9.15 \times 10^{-7}$	$< 10^{-3\dagger}$
F	A	$1.08 \times 10^{-7}$	$< 10^{-3\dagger}$
F	S	$9.15 \times 10^{-7}$	$< 10^{-3\dagger}$
R	N	$9.15 \times 10^{-7}$	$< 10^{-3\dagger}$
R	A	$1.89 \times 10^{-7}$	$< 10^{-3\dagger}$
R	S	$9.15 \times 10^{-7}$	$< 10^{-3\dagger}$
D	N	$5.09 \times 10^{-7}$	$< 10^{-3\dagger}$
D	A	$2.72 \times 10^{-7}$	$< 10^{-3\dagger}$
D	S	$5.09 \times 10^{-7}$	$< 10^{-3\dagger}$

<sup>†</sup>significance level to small to calculate.

**Table SI-3:** Details for the DFA analysis carried out on the array normalized fractional pre-processed values for the observations at maximum concentration levels.

Discriminant Function	Eigenvalue ?	Contribution (%)	Cumulative Contribution (%)	<i>p</i> -value	Sensors Contributing
$a_1$	172.81	52.4	52.4	$< 10^{-7\dagger}$	A, C, E, F
$a_2$	76.79	23.3	75.7	$< 10^{-7\dagger}$	A, C, D, F
$a_3$	74.10	22.4	98.1	$< 10^{-7\dagger}$	B, D
$a_4$	5.80	1.8	99.9	$0.99 \times 10^{-10}$	A, C, F
$a_5$	0.34	0.1	100.0	0.091	B

<sup>†</sup>significance level to small to calculate.

**Supporting Information****Table SI-4:** Details for the DFA analysis carried out on the array normalized fractional pre-processed values for the combined maximum and diluted concentration samples.

<b>Discriminant Function</b>	<b>Eigenvalue ?</b>	<b>Contribution (%)</b>	<b>Cumulative Contribution (%)</b>	<b>p-value</b>	<b>Sensor Contributing</b>
$a_1$	<b>10.24</b>	<b>65.2</b>	<b>65.2</b>	$< 10^{-7\dagger}$	<b>C, D, E</b>
$a_2$	<b>2.51</b>	<b>16.0</b>	<b>81.2</b>	$< 10^{-7\dagger}$	<b>B, C, E</b>
$a_3$	<b>1.48</b>	<b>9.4</b>	<b>90.6</b>	$< 10^{-7\dagger}$	<b>B, F</b>
$a_4$	<b>1.28</b>	<b>8.2</b>	<b>98.8</b>	$4.0 \times 10^{-9}$	<b>A, B, D, F</b>
$a_5$	<b>0.18</b>	<b>1.2</b>	<b>99.97</b>	<b>0.042</b>	<b>B</b>
$a_6$	<b>0.00</b>	<b>0.03</b>	<b>100.0</b>	<b>0.614</b>	<b>A, B</b>

<sup>†</sup>significance level too small to calculate.

**REFERENCES for Supporting Information**

- (1) Grimm, L. G.; Yarnold, P. L. e. *Reading and Understanding Multivariate Statistics*; American Psychological Association, 1995.
- (2) Kaiser, H. F. *Ed. Psy. Measurement* **1960**, *20*, 141-151.

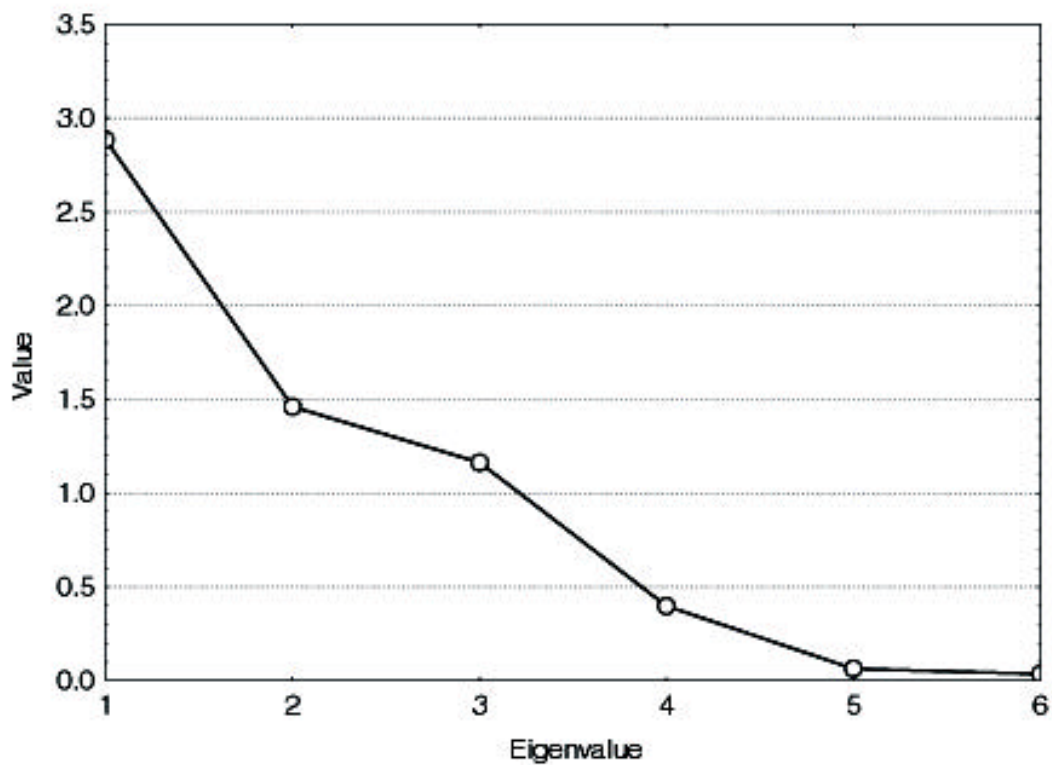


Figure SI-1a

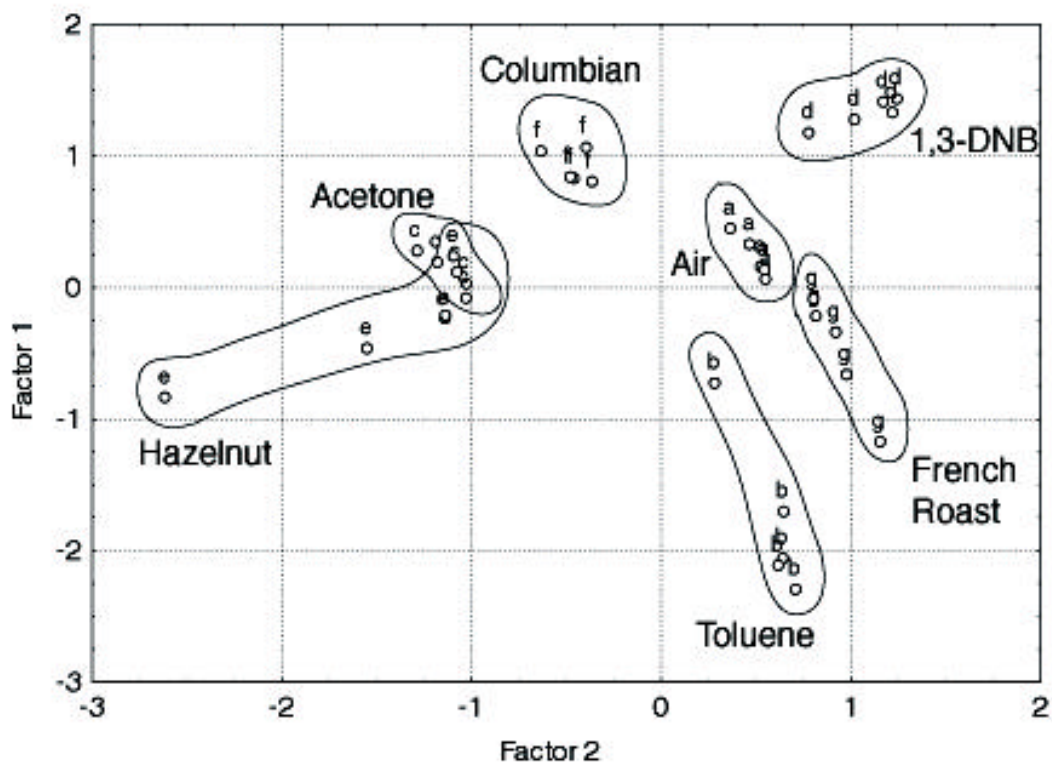


Figure SI-1b

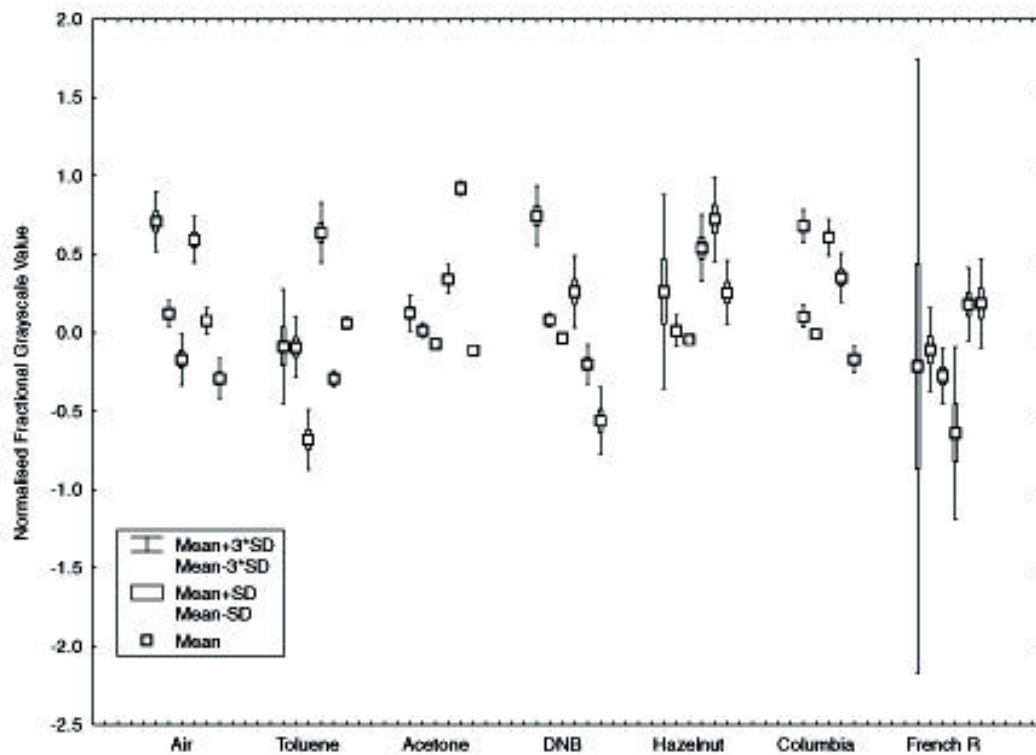


Figure SI-2